Transport and Mechanical Aspects of All-Solid-State Lithium Batteries

Grayson Deysher[+, a], Phillip Ridley[+, b], So-Yeon Ham[a], Jean-Marie Doux[b], Yu-Ting Chen[a], Erik A. Wu[b], Darren H. S. Tan[b], Ashley Cronk[a], Jihyun Jang[b], Ying Shirley Meng[b, c, *]

[a] Program of Materials Science and Engineering, University of California San Diego, La Jolla, CA 92093, United States.

[b] Department of NanoEngineering, University of California San Diego, La Jolla, CA 92093, United States.

[c] Pritzker School of Molecular Engineering, The University of Chicago, Chicago, IL 60637, United States

* shirleymeng@uchicago.edu

Abstract:

All-solid-state batteries (ASSBs) have been promoted as a highly promising energy storage technology due to the prospects of improved safety and a wider operating temperature range compared to their conventional liquid electrolyte-based counterparts. While solid electrolytes with ionic conductivities comparable to liquid electrolytes have been discovered, fabricating solid-state full cells with high areal capacities that can cycle at reasonable current densities remains a principal challenge. To overcome these challenges, a quantitative and in-depth understanding of the phenomena governing ionic and electronic transport limitations within the cathode composite, in addition to mechanical aspects arising from significant volume changes associated with Li metal anodes (including anode-less cell designs) are needed. Such understanding can be obtained from proper electrochemical measurements described herein. In this review we seek to highlight solutions to these existing challenges and several directions for future work are proposed.

1 Introduction: Current Bottlenecks for All-Solid-State Batteries

In pursuit of safer, more energy dense, and longer-lasting rechargeable batteries, recent research efforts have concentrated on developing all-solid-state battery (ASSB) technologies to meet next-generation device requirements. Extensive research in solid-state ionics has explored various material classes that can deliver high ionic conductivities (> 10 mS at room temperature), with some, such as $Li_{10}GeP_2S_{12}$ (LGPS) and $Na_{2.88}Sb_{0.88}W_{0.12}S_4$, that even surpass those of common liquid organic electrolytes [1,2]. As a result of these efforts, numerous solid-state electrolytes (SSEs) have been discovered, including many oxides, sulfides, and halides [1–8]. However, achieving practical cell performance remains an elusive goal. Thus, attention and research efforts must shift towards addressing the principal bottlenecks limiting the performance of ASSBs.

Low current densities (< 2 mA cm^{-2}) and low areal capacities (< 2 mAh cm^{-2}) are often reported in literature [1,6,9–28], as illustrated in Figure 1. There are few outlying examples that demonstrate higher and more industrially relevant areal capacities; one such example is the work of Yong-Gun Lee *et al*., where a $LiNi_{0.9}Mn_{0.05}Co_{0.05}O_2$ (NMC) | Li_6PS_5Cl (LPSCl) | Ag-C pouch cell with a high capacity of 6.8 mAh cm^{-2} was cycled at 3.2 mA cm^{-2} [24]. Despite this noteworthy electrochemical performance, key cycling and fabrication parameters reveal that elevated temperature (60°C), sub-micrometer sized SSE particles, and isostatic pressure-based fabrication steps are needed to enable such a cell with large cathode areal capacity at such high current density. Similarly, another prominent example by Tan *et al*. [25], demonstrated 80% capacity retention over 500 cycles at 5 mA cm^{-2} in a NCM811| LPSCl | μSi full cell. Although the areal capacity used in this work was relatively high (2 mAh cm^{-2}) compared to other reports in the literature, the cathode capacity utilization was still poor (<50%), resulting in limited energy density. These examples suggest that transport kinetics in the cathode composite are a major challenge, particularly at room temperature. Both Li^+ and e^- transport can be hindered in these composites due to various reasons outlined in this review, such as cathode particle volume change and subsequent void formation. When charge transport is limited, the redox capability of the electrode is also limited, thus limiting the effective capacity utilization. To address these issues, cathode composite engineering is a critical area requiring further exploration. New knowledge in this area is needed to properly assess the limitations of cathode composites and to potentially enable practical ASSB performance at ambient temperatures.

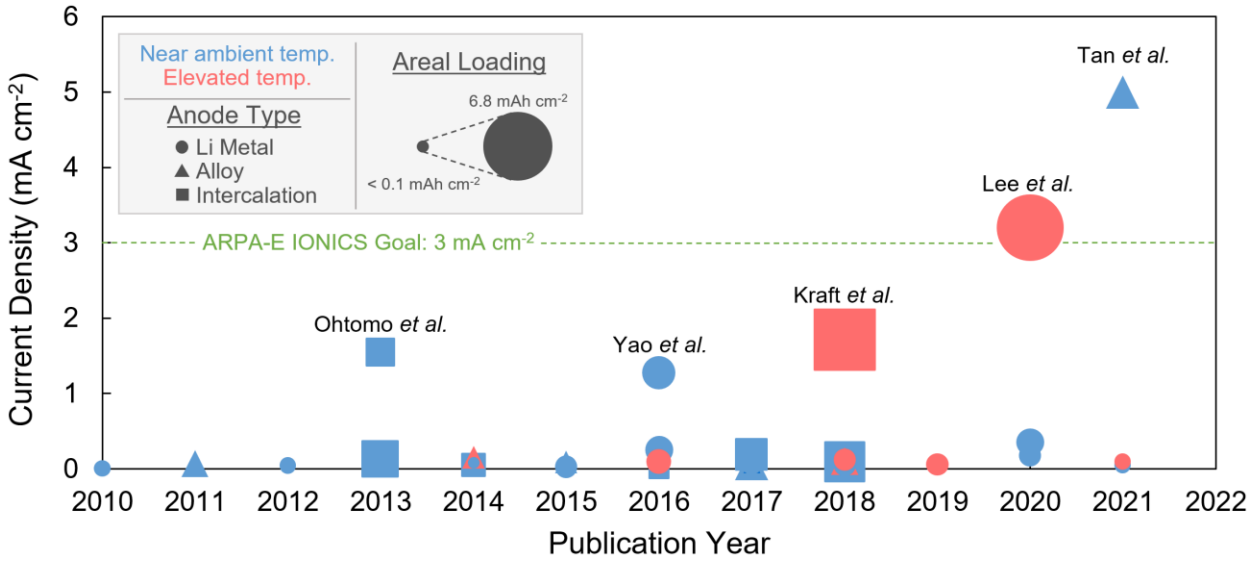

Figure 1. Survey of existing literature revealing the performance limitations of ASSBs. Low current densities and low areal loadings (denoted by the size of the point) are common. The ARPA-E IONICS project goal of 3 mA cm^{-2} from 2016 is denoted by the green dashed line for reference.

Apart from transport limitations associated with cathode composites, Li metal anodes also contribute to the limited areal capacities and current densities reported by recent studies. Although batteries containing a Li metal anode offer the most promising energy density, they also face their own limitations regarding current density. Generally, the critical current density (CCD) can be defined as the maximum operating current density which can be applied before cell short-circuiting

is induced. This short-circuiting effect has been attributed to the propagation of Li metal dendrites along the grain boundaries of the SE, which has been demonstrated for $Li_7La_3Zr_2O_{12}$ (LLZO) [29,30], and has recently been attributed to the bandgap reduction of the SSE at its grain boundaries, which facilitates electron transport and subsequent Li-metal deposition at higher current densities [31]. Partly due to this factor, as shown in Figure 1, the highest room temperature current density used for Li metal cells is still less than 2 mA cm^{-2}. Moreover, higher current densities have been reported for Li metal symmetric cells compared to full cell configurations over the past decade [28,30,32–62]. It is evident that higher current densities achieved in the symmetric cell configuration cannot be reproduced in full cell formats (Figure 1). Understanding this discrepancy remains a challenge, though we will propose a hypothesis to this issue, which relates to the significant cell volume change experienced in full cells that is not experienced in symmetric cells.

Beyond enabling practical areal capacities and current densities, more work is needed to understand and predict the long-term cycle performance of ASSBs. As such, both experimental and computational studies have pivoted towards enhancing interfacial stability at the electrolyte-electrode interfaces, seeking to minimize electrolyte oxidation or reduction [63]. However, it is still challenging to achieve wider electrochemical stability windows without sacrificing ionic conductivity. Moreover, some of the commonly used protocols for characterizing the electrochemical properties of solid electrolytes have flaws that need to be addressed to ensure the accurate determination of material properties, as will be discussed later in this review. In addition to electrochemical stability, mechanical stability is an important factor for long-term cyclability. However, there is a significant knowledge gap in the understanding of the mechanical properties of emerging solid electrolyte materials and their composites. Therefore, more work in these key areas is needed, as these limitations are roadblocks to the deployment of ASSB technologies.

2 Kinetic Transport Limitations in the Cathode Composite

Ion conduction within solid materials is governed by Equation 1, where σ_q is conductivity, n_q is the charge carrier density, q is the charge of the carrier, and μ_q is the mobility of the carrier. n_q and μ_q are dependent on the material composition and crystal structure; the product of these two values should be maximized for Li^+ to achieve high ionic conductivities. When considering the conductivity within a battery, the conductivity can be calculated based on the value obtained from a simple resistance measurement (Equation 2), where t is the thickness of the sample, R is the measured resistance, and A is the cross-sectional area of the sample. This is a fundamental tool for assessing any ASSB or its components. Lastly, as demonstrated in Figure 1, higher temperatures are frequently needed to enable higher areal capacities. This is due to the Arrhenius relationship between ionic conductivity and temperature, as shown in Equation 3, where σ_0 is a pre-exponential factor and E_a is the activation energy. Ionic conductivities increase with temperature, which lowers the resistance within the battery and lowers the overpotential according to Ohm's law (V = IR). This enables more capacity to be obtained before reaching the voltage cutoff. These three equations provide the foundation for understanding the challenges facing ASSBs and provide invaluable insight into how to solve them.

$$\sigma_q = n_q \times q \times \mu_q \qquad \text{Equation 1.}$$

$$\sigma = \frac{t}{R \times A} \quad \text{Equation 2.}$$

$$\sigma = \sigma_0 \times e^{-\frac{E_a}{RT}} \quad \text{Equation 3.}$$

2.1 Capacity Utilization

To ensure utilization of all cathode-active particles, each particle must transport ions and electrons to the SSE matrix and current collector, respectively. Unfortunately, the electronic and ionic conductivities of cathode materials tend to be relatively low [64,65], which means that composite mixtures comprised of active material, solid electrolyte, and electronically conductive carbon additive must be used. In a simple thought experiment, if there is a finely dispersed ionically/electronically conductive network of SSE/carbon particles in which every cathode particle is surrounded by SSE/carbon, then the ions/electrons must only travel through one active material particle before reaching the fast-conducting SSE/carbon. This will increase the capacity utilization and high-rate capabilities due to the lower overpotential of the cell, allowing for more capacity to be utilized before the voltage limit is reached. Conversely, in poorly dispersed composites where some active material particles are isolated from the SSE/carbon, the resistance will be higher and thus the capacity utilization will decrease.

Unlike liquid electrolytes, which can readily flow to make good interfacial contact with every cathode particle (thus providing ample ion transport), SSE particles obviously cannot. Consequently, the mixing method and resultant morphology of the fabricated cathode composite used in ASSB systems becomes critical for achieving good battery performance. Thoughtful morphological design is required to optimize the distribution and interfacial contact area between all three components in the cathode composite. Namely, sufficient ion and electron transport is needed to enable both higher current densities and areal capacities. Therefore, morphological parameters such as the size of both the electrolyte and cathode particles should be optimized, in addition to the total porosity of the composite electrode. Recent microstructural modeling revealed the impact of electrode porosity on cathode particle utilization, where it was detailed that less than 20% porosity is needed to achieve full capacity utilization at higher cathode weight percentages (>55%) in the composite [66].

Shi *et al.* recently developed a 3-dimensional cathode composite model [67], in which the particle size of the SSE was varied along with the cathode : SSE ratio (Figure 2a). From the initial input parameters, a model of the ion conduction network (SSE particles) was created to qualitatively evaluate the cathode particles being utilized, whereby only cathode particles in contact with the SSE are considered active. A quantitative analysis was conducted to obtain a numerical trend for cathode particle utilization as a function of both the SSE particle size and cathode loading (Figure 2b). These modeling results show that smaller SSE particles and a lower cathode loading offer higher utilization, because smaller SSE particles offer a more continuous, homogeneous, and finely dispersed ion conduction network throughout the composite. Additionally, a lower cathode to SSE ratio enables a higher volume fraction of the composite to be active with the SSE network, which then results in a lower probability of cathode particles being isolated from contact with the SSE. However, while this work examined the effect of varying the

SSE and cathode morphological parameters, the effect of electronically conductive additives was not evaluated.

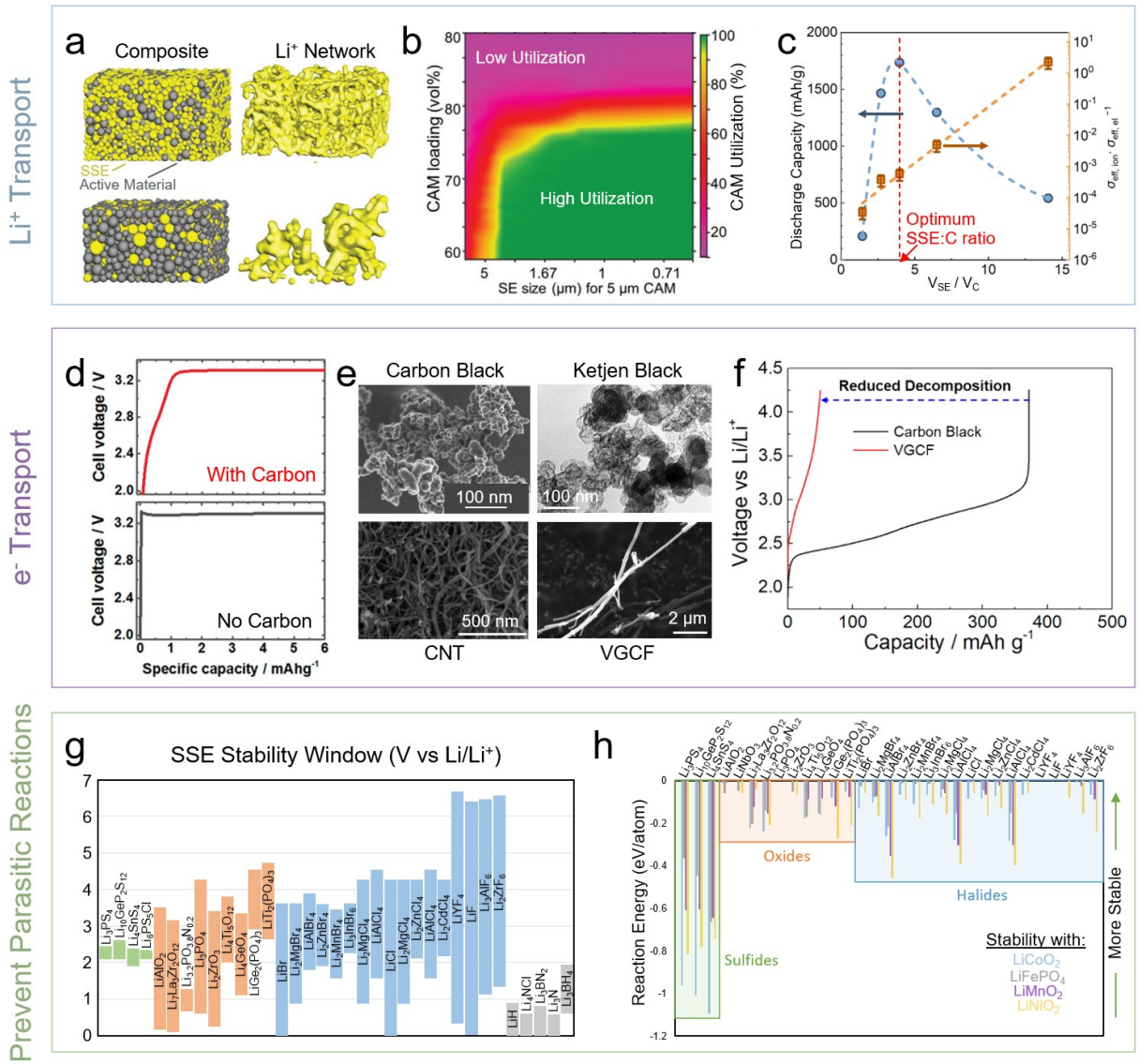

Figure 2. Methods to optimize the electronic and ionic transport within the cathode and considerations for SSE electrochemical stability. **a)** & **b)** SSE-to-cathode particle size ratio effects on cathode capacity utilization [67]. **c)** Optimizing the composite ratio to maximize both ionic and electronic transport within the cathode [68]. **d)** Effect of carbon addition (Adapted with permission from [69] (Copyright 2017 American Chemical Society)) and **e)** various morphologies of common carbon additives [70] (CNT: carbon nanotubes, VGCF: vapor-grown carbon fibers). **f)** Effect of carbon morphology on decomposition kinetics (Adapted with permission from [71] (Copyright 2019 American Chemical Society)). **g)** Electrochemical potential windows for several material classes of solid electrolytes (Adapted with permission from [72] (Copyright 2020 American Chemical Society)). **h)** SSE reaction energies with a few common cathode materials (Adapted with permission from [73] (Copyright 2016 American Chemical Society)).

In addition to possessing a finely dispersed and ionically conductive network, electron transport within the cathode composite must also be considered. It is imperative to consider the effect of conductive carbon additive loading and morphology on the cathode particle utilization.

When using liquid electrolytes, the active material is mixed in a slurry with carbon and casted, resulting in a well-dispersed electronically conductive network. This network enables electrons to easily reach all available cathode particles, thereby enabling them to participate in the desired redox reactions. The cast electrode pores are then infiltrated by the liquid electrolyte, which does not affect the existing carbon network. On the other hand, in ASSBs the cathode particles must be mixed with both carbon and the SSE. Due to the mixing of these solid components, it is more challenging to achieve a uniform distribution of both the carbon and SSE to ensure that all active material particles have sufficient electronic transport to the current collector. Therefore, to maximize cathode particle utilization, additional optimization is required and will depend on the type of mixing methods, conductive additive morphology, and the percentage of both SSE and carbon in the composite.

An ideal scenario to study the effects of the carbon and SSE components is to use a cathode material that is both ionically and electronically insulating, therefore isolating the effects of the electronically- (carbon) and ionically- (SSE) conductive additives. It can be quite difficult to determine whether a cell with lower cathode particle utilization suffers from electronic or ionic transport limitations, or both. Limited electronic or ionic transport can both increase cell impedance, which increases cell polarization and limits the usable capacity. Simply evaluating the rate performance of a particular composite design cannot provide the information necessary to determine the rate-limiting transport mechanism. Therefore, various composite ratios need to be assessed to evaluate this effect on the cathode utilization. Recent work has demonstrated the effect of carbon and SSE volume fractions within the composite for an insulating sulfur cathode [68]. Figure 2c shows the resulting cathode capacity for a fixed amount of sulfur as the SSE:carbon ratio was varied. The results show that there is an optimal point of maximum capacity, where either increasing or decreasing the SSE:carbon ratio negatively affects the utilization, due to either limited ionic or electronic transport. While the exact value of this optimal point will vary depending on the respective cathode's material properties, morphology, and loading, the same approach can be applied to other systems, effectively serving as a cathode composite design platform.

2.2 Morphology of Electronically Conductive Additives

While electronically conducting additives are essential for cathode particle utilization, they also provide sites where the SSE can be oxidized, if the oxidative potential of the cathode is higher than the upper stability limit of the SSE. This is a common occurrence, as sulfides are the most commonly used SSE materials due to their high ionic conductivities, although their oxidative stability is limited and well below the potentials of many cathode materials (Figure 2g) [72]. This has been shown in an In | LGPS | $LiCoO_2$ solid-state battery system (Figure 2d), where an additional voltage offset appeared before the voltage plateau at 3.3 V vs. In/InLi, which does not occur in the carbon-free equivalent cathode composite due to the minimal 2-dimensional interfacial area (current collector) at which SSE oxidation can occur [69]. Therefore, when using SSEs that are expected to oxidize, the carbon weight percentage used, surface area, and morphology are important considerations when aiming to maximize electronic transport and cathode particle utilization but minimize cell impedance growth from electrolyte oxidation in the composite.

Moreover, various types of carbon additives have been studied in the cathode composite, such as carbon black, Ketjen black, carbon nanotubes, and vapor-grown carbon fibers (VGCF) (Figure 2e) [70]. The effect of their varying surface area can be seen in Figure 2f, where high surface area carbon black resulted in significantly more electrolyte oxidation and interfacial impedance during charging than a lower surface area carbon, such as VGCF. Here, the LPSCl electrolyte was used as the cathode material and charged to 4.25 V vs Li/Li^+, which is higher than its oxidative stability limit of 2.1 V vs Li/Li^+ [71]. Therefore, while electronic transport to the cathode particles should be maximized to enable their utilization and promote a more homogeneous current distribution, the interfacial contact area between the carbon and the SSE should be minimized in these composites to decrease the undesirable SSE oxidation. SSE oxidation products may exhibit significantly different mechanical properties compared to the pristine SSE, which may cause additional or exacerbated detrimental effects, such as increased contact loss upon repeated cycling and subsequent capacity fade [74]. To address these challenges, optimized carbon morphologies should be developed and evaluated to enable high utilization, good rate capability, while minimizing cell impedance growth at the cathode-SSE particle interface when charging beyond the limit of SSE oxidative stability. Additionally, many SSE materials have the tendency to react chemically with their neighboring cathode particles as shown by the negative reaction energies in Figure 2h [73]. Other SSE materials should thus be explored that are less chemically reactive with the cathode materials and have higher oxidative voltage limits, which can eliminate or minimize the issues regarding carbon contact with the SSE. While the highest ionic conductivities are currently still exhibited by sulfides [1,2], there has been significant progress recently on improving the ionic conductivity of chlorides [73,75–77], which potentially offer a more stable long-term solution for achieving higher voltage (and coating-free) cathode composites.

2.3 Cathode and SSE Interfacial Contact Optimization

Although a continuous ion conduction network within the cathode composite is needed for battery operation, practical considerations like energy density should not be ignored. Bulky micron-sized SSE particles effectively limit the attainable cathode utilization when using practical areal capacities and high cathode weight percentages (Figure 2a,b) [67], and limit both the volumetric and gravimetric capacity of the cathode composite. One strategy to circumvent the limitation imposed by SSE particle geometry involves the dissolution of the SSE in a suitable solvent, followed by an infiltration of that solution into a casted cathode. This has been previously demonstrated using LPSCl [78], where the utilization of the cathode ($LiCoO_2$) and anode (graphite) were significantly improved, and close-to-theoretical specific capacities of 141 and 364 mAh g^{-1} were achieved, respectively. Remarkably, this was accomplished while the amount of SSE in the composite was greatly reduced (~10 and ~20 wt.% in the cathode and anode, respectively). This is a promising strategy that merits further exploration, but ensuring uniform wetting of the electrode is not trivial using this approach, particularly at high areal loadings where infiltration through thick electrodes becomes challenging.

A second strategy that has been reported can resolve the challenges of cathode wetting entirely. Instead of infiltrating the cathode *via* solution processing, the SSE can be coated directly onto the individual cathode particles before the electrode is fabricated [3]. Using a similar solution process as the infiltration method, an SSE coating can be precipitated onto the surfaces of each individual

cathode particle. These coatings can be on the order of hundreds of nm, which greatly decreases the amount of inactive material in the composite compared to the conventional mixture of cathode and SSE particles, thus drastically improving energy density. This strategy also addresses the need for good interfacial contact between the cathode and the SSE. This increase in contact enables improved and more uniform ion transport across the cathode-SSE interface, which improves capacity utilization by decreasing the interfacial impedance. Additionally, the SSE tortuosity can be decreased, which effectively shortens the length t in Equation 2.

While SSE infiltration and coating strategies can be highly useful for improving cathode utilization, they are only applicable to SSEs that can be dissolved and then subsequently precipitated, all while retaining their original composition, structure, and properties. Additionally, these strategies might exacerbate cathode-electrolyte interphase (CEI) formation due to the increased contact area. There have been no examples yet that successfully demonstrate this strategy for a solid electrolyte with oxidative stability > 3 V vs Li/Li^+. Lastly, although SSE coating methods can provide sufficient ion transport, incorporating electronic transport can be challenging due to the electronically insulating layer created by the SSE coating.

Beyond minimizing the amount of inactive SSE in the cathode composite, the thickness of the SSE separator layer should also be controlled to reduce the inactive volume and weight of the battery to enable higher energy densities. Previous work has included the development of novel casting procedures for common electrolytes like LPSCl [23,24,79,80]. These methods involve the use of solvents, polymer binders, and slurry mixing to disperse the SSE particles such that a thin (< 50 μm) layer can be cast on top of an anode or cathode layer. Alternatively, the SSE can be cast onto a polymer sheet. The free-standing SSE film can then be peeled off and placed on top of the electrode during cell fabrication. While casting the SSE directly onto an electrode allows for thinner layers to be used, the uniformity of a free-standing film will likely be more controllable compared to a cast SSE layer as it can mold to the flat surface of the polymer sheet, compared to the rough surface of a cast electrode. These methods can both drastically reduce the dead weight of the SSE component of the battery compared to commonly used pellet-cell architectures that utilize ~ 0.5 mm thick SSE separator layers [26,27,67,68,81–85]. As new electrolytes are developed, such as halides or borohydrides, solvent compatibility will be an important factor when considering their industrial practicality.

3 Mechanical Failure Mechanisms

3.1 Cathode Particle Engineering and Design

At the cathode particle level, the biggest mechanical challenge originates from the volume change experienced by the particles during charging and discharging such as NMC materials (1-3%) [86]. This volume reduction results in a loss of contact stemming from the formation of interparticle voids between the active material and SSE particles (Figure 3a). This issue, not observed with liquid electrolytes, occurs because of the inability for the SSE to flow and maintain good contact with the cathode particles as their volume changes. This loss of contact results in decreased cathode utilization due to restriction of ion transport across the formed voids. This phenomenon was recently reported, and it was demonstrated that after a cell experienced

significant capacity fade over the first tens of cycles, much of this lost capacity could be recovered by simply re-pressing the cell with sufficient pressure (370 MPa) [87]. Re-pressing the cell collapses the voids and reforms the interfacial contact between the cathode and SSE particles. However, this is not at all a practical strategy for enabling long cycle-life, because it would require routine disassembly of the solid-state cells.

When diagnosing the origins of capacity fade in solid-state cells, it can be challenging to decouple the contributions of various failure mechanisms. Previously, capacity fade has been attributed to CEI formation from oxidation of the SSE, but while the CEI is certainly an issue due to the formation of insulating byproducts and subsequent increase in cell polarization, the majority of CEI formation is likely limited to the first cycle [88]. As an example, complete oxidation of LGPS results in products such as GeS_2, P_2S_5, and S [89]. All of these CEI components have reasonably large band gaps (2.3, 2.6, and 2.7 eV, respectively, from Materials Project [90]) indicating that they are poor electron conductors. Without facile electron transport, the CEI should quickly passivate. Therefore, after the first cycle, it is likely that any subsequent capacity fade observed previously [1] is not due to additional CEI formation, but rather primarily due to mechanical effects such as void formation and contact losses between cathode and SSE particles. Recent work has experimentally observed this capacity fade mechanism for the Li_3PS_4 electrolyte and NMC cathode particles [91]. In these instances, the choice of characterization techniques becomes important as electrochemical cycling data alone will not provide much insight into issues originating from cathode volume change. Additional techniques like focused-ion beam (FIB) milling that can be conducted under stack pressure, and paired reconstruction should be used to adequately assess the composite morphology changes.

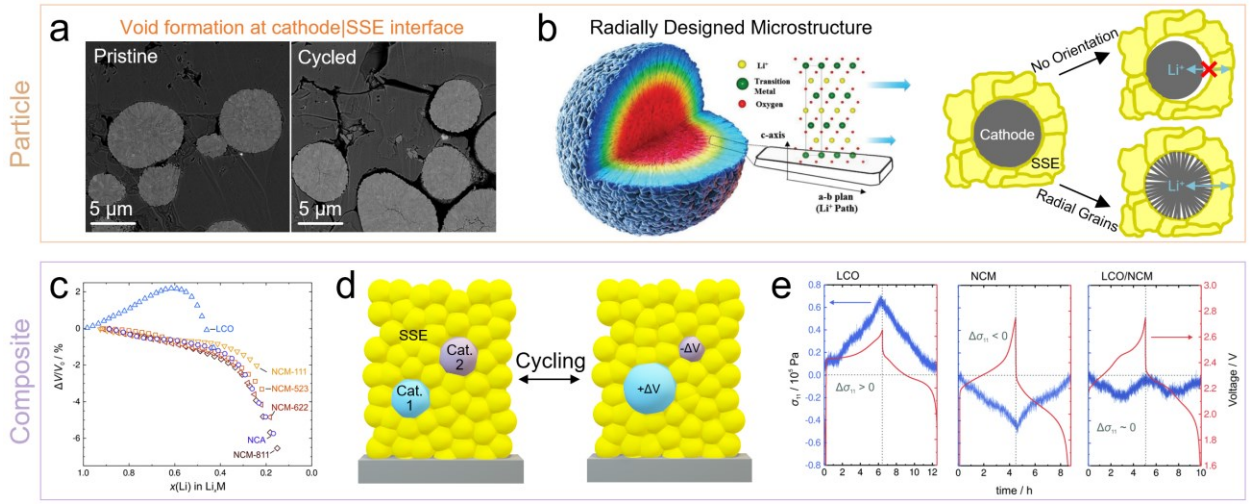

Figure 3. Common mechanical failure mechanisms observed in ASSBs. **a)** Void formation between the cathode and the SSE due to the repeated expansion and contraction of cathode particles. **b)** Radially oriented grains within the cathode particles to mitigate the loss of contact with the SSE (Reproduced with permission from [92] (Copyright 2019 John Wiley and Sons)). **c)** Volume expansion of different cathode materials during cycling (Reproduced with permission from [86] (Copyright 2018 Royal Society of Chemistry)). **d)** & **e)** Mixing cathode materials with different volume change trends during lithiation to minimize the overall

composite volume change (Reproduced with permission from [86] (Copyright 2018 Royal Society of Chemistry)).

Although the volume change of most layered oxide cathode materials is inevitable due to ion (de)intercalation, microstructure design can potentially offer a route to control this volume change in such a way to maintain good interfacial contact with the SSE. This approach has been used previously to address the pulverization of cathode particles in liquid electrolytes after prolonged cycling [92]. This strategy involves growing the grains of a secondary cathode particle radially outward along a particular crystallographic direction. Layered cathode materials often experience volume change along one primary crystallographic direction [93–96]. Therefore, for these materials, if the crystallographic direction pointing radially outward from the particle is not the one that undergoes significant volume change, the particle should not shrink radially. Figure 3b shows the expected benefit of this type of volume change control with respect to ASSB systems. Rather than randomly oriented grains in a typical secondary particle (which contract radially and therefore result in void formation), a radially oriented microstructure could mitigate radial particle shrinkage. This method should allow the secondary particle to retain most of its interfacial contact with the surrounding SSE, thus enabling improved capacity retention. However, this strategy still needs to be investigated and validated experimentally in ASSB systems.

The summation of the effects of individual cathode particle volume change results in a composite that will experience an overall volume change. To minimize this effect, a method to compensate for the volume change must be developed. As shown in Figure 3c, two common Li cathode materials $LiCoO_2$ (LCO) and NMC have opposite trends for volume change during delithiation and lithiation [86]. If these cathode materials are mixed in the proper ratios within the composite cathode, then the amount of volume expansion that one experiences can be offset by the volume shrinkage of the other (Figure 3d), resulting in zero net volume change at the composite level. This strategy has been verified experimentally with these two cathode materials (Figure 3e) [86]. To determine whether the cell was expanding or contracting, the stack pressure of the cell was monitored during cycling. $Li_4Ti_5O_{12}$ was used as the anode due to its negligible volume change during cycling [97], thereby isolating the volume change to only the cathode side of the cell. The mixture of the two materials indeed resulted in minimal pressure change, which can be attributed to the minimized net volume change in the cathode composite. This strategy has so far only been demonstrated for LCO and NMC, and therefore more work is needed in this area to further validate this strategy, especially with low SSE weight fractions.

3.2 Li Metal Anode Volume Changes

When it comes to a full cell architecture, the anode volume expansion contribution is not negligible. In fact, the volume change experienced at the anode is very significant for Li metal or anode-less designs. Interestingly, compared to plated Li metal in conventional liquid electrolytes, electrochemically formed Li metal in solid-state cells exhibits a dense morphology due to the SEI passivation for many commonly used SSEs, like bulk Li metal (Figure 4a). This dense morphology results in very predictable thickness changes of the anode during plating and stripping. Thus, a simple thought experiment can be designed to obtain an estimate for the order of magnitude of volume change being experienced by a full cell. For example, if NMC811 is used as the cathode in an anode-less configuration, then although the NMC811 will contract during charging, the Li

metal that gets plated on the anode side will expand by an order of magnitude more (about 5 µm per 1 mAh cm^{-2} of plated Li) (Figure 4b). This cell volume expansion becomes even more significant at higher areal loadings, as the lithium reservoir and subsequent amount of plated Li is increased. Furthermore, if the ASSB is constructed with the commonly used fixed-gap configuration where the distance between the current collectors is constrained, then the stack pressure exerted on the cell will increase due to the volume expansion and thickness constraint. This would become problematic as higher stack pressures have been shown to result in mechanical shorting of Li metal cells [98].

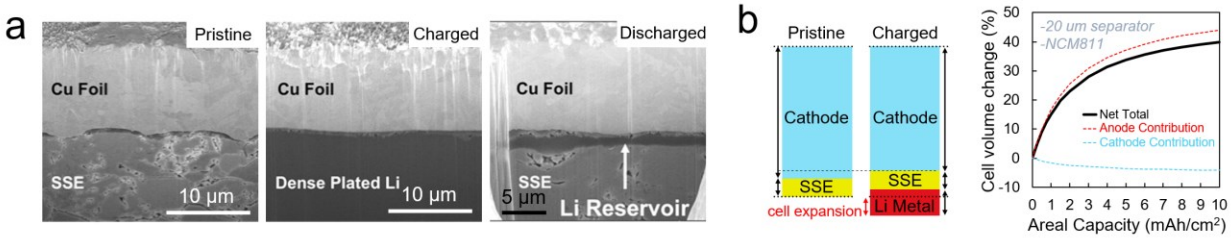

Figure 4. Cell volume expansion in Li-metal ASSBs. **a)** Observation of dense Li plated in ASSBs. **b)** Evaluation of total cell volume change during cycling for Li metal full cells.

A possible solution toward overcoming high-pressure induced mechanical shorting is to explore alloy-based materials on the anode side of the cell. In addition to offering a potential mitigation strategy for the electrochemical formation of dendritic structures, alloy-based anodes might also alleviate the mechanical shorting experienced in Li-metal cells. Like many other metals, Li metal can undergo creep when a sufficient load is applied to it [99], which can result in cell shorting. Moreover, creep is known to occur more rapidly near the melting temperature of a material [100,101]. As such, while the melting temperature of Li is 180.6 °C, the melting point of some Li-alloys such as (Li)Si and (Li)Sb are significantly higher (> 592 °C [102] and > 466 °C [103], respectively). Therefore, it is expected that the propensity for a Li-alloy to creep is far lower than that of pure Li metal. Although Li-alloys experience significant volume expansion (> 300% for Li-Si) during lithiation [25], they should be able to withstand higher operating pressures compared to Li metal, due to these more favorable mechanical properties. The stack pressures reported for these alloy type anode materials are 5-150 MPa for Li-In [104] and 50 MPa for Li-Si [25], which are significantly higher than the operating range of Li metal anode cells (1-7 MPa). Additionally, this approach has an added benefit when using a fixed-gap design. As demonstrated recently [25], Si expands during lithiation in a solid-state cell which should result in increased stack pressure. Interestingly, after delithiation of the Si, it does not fully shrink back to its original thickness, therefore retaining some of the previously increased stack pressure. This higher stack pressure is likely to improve the capacity retention on the cathode side due to the possible mitigation of void formation. In this instance, a fixed-gap configuration is desirable.

Although alloying materials may show promise in solid-state cells, the Li metal anode remains desirable, especially in anode-less configurations where it can theoretically store infinite Li and provides the lowest possible reduction potential (highest cell voltage and thus higher energy density). Its use as an anode in ASSBs is still achievable if the stack pressure is controlled and remains relatively low (< 5 MPa) during cell cycling. The relationship between external pressure

and Li metal cell performance has been widely explored. Notably, Wang *et al.*[105] first defined the "critical stack pressure" for operating solid-state cells, where their work demonstrated that Li/LLZO/Li symmetric cells required an applied stack pressure above a certain critical stack pressure, otherwise significant cell polarization was observed. This polarization was attributed to void formation when the stripping of Li was faster than the Li transport to the interface via creeping caused by the applied stack pressure. Kasemchainan *et al.*[106] differentiated the critical plating and stripping currents in a $Li/Li_6PS_5Cl/Li$ symmetric cell. The critical stripping currents were 0.2 (3 MPa) and 1.0 mA cm^{-2} (7 MPa), whereas the critical plating currents were 2.0 mA cm^{-2} at both low and high pressures. This indicates that the Li stripping step is the bottleneck of void formation, and thus a precise pressure and current density should be applied during the Li stripping to avoid void formation and subsequent cell polarization. At stack pressures of 1-7 MPa, Li metal undergoes plastic deformation and creep considering its yield strength is ~0.8 MPa [107]. Creep can then cause internal shorting through ceramic electrolytes due to Li creeping into surface cracks at the anode/electrolyte interface [108]. The localized strain at the end of the cracks would be formed faster with higher current densities, which lead to stress accumulation at the crack tip.

Maintaining lower pressures in the case of Li metal cells requires the design of new cell casings that can account for volume changes while maintaining a constant stack pressure. There are two possible designs to achieve this, with the first utilizing springs in the cell casing that can apply pressure to the ASSB cell stack. The force response of a compressed spring (cell volume expansion) can be simply expressed using Hooke's law: $F = -kx$, where F is the force required to compress or elongate the spring, k is the spring specific constant, and x is the spring's displacement. If the chosen spring has a suitable spring constant, then the desired pressure can be applied on the pristine cell by setting its displacement. After charging, depending on the areal capacity and number of layers (Figure 4b), the ASSB can be expected to expand by tens to hundreds of microns (Figure 5). This amount of expansion should not significantly affect the force response of the spring, as small changes in spring displacement would result in minimal changes to the force applied by the spring (and corresponding pressure, as the area is constant).

A second, more complex design solution may involve pressurization of the entire stack, under either pneumatic or hydraulic isostatic pressure. The pressure could be controlled externally, and therefore be maintained constant throughout battery cycling. This method has the advantage of more precise pressure control compared to a spring-loaded design (where the applied force must be controlled by the spring constant and its displacement). Moreover, spring fatigue and failure may become an issue after long-term use from extended cell cycling. However, one drawback is the need for a pressurized vessel at the pack level to contain the battery stacks. While an applied stack pressure in the range of one to a few MPa can be considered high, it is still approximately one order of magnitude lower than pressurized hydrogen tanks used in fuel-cell vehicles, which are often 70 MPa for passenger cars, as specified by the United States Department of Energy [109]. Therefore, careful design may be able to minimize the amount of gas or fluid needed to adequately pressurize the battery pack pressure system. Hydraulic pressure offers a higher level of safety compared to pneumatic pressure, although there will be an energy density tradeoff, as any fluid will add more weight to the battery pack. Similarly, it is worth noting that both spring-loaded and hydraulic/pneumatic casing designs will inevitably impact the energy density of the system as well

as the design constraints for any devices implementing them, like electric vehicles. Therefore, when assessing the suitability of Li-metal ASSBs for various commercial applications, the overall energy density of the pack needs to be carefully considered.

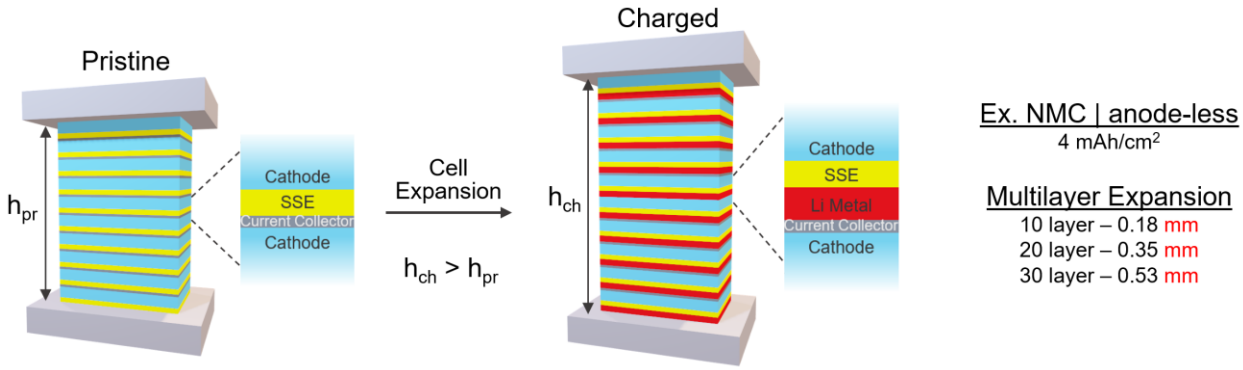

Figure 5. Cell volume expansion in multilayer Li-metal ASSBs. The magnitude of volume expansion experienced by Li metal cells increases linearly with the number of layers. New cell designs are needed to accommodate these macro-scale volume changes.

When designing the anode, some differences can be observed compared to the cathode composite. First, the Li metal anode only has a 2-dimensional interface with the SSE separator layer, as there is no SSE mixed in with the anode. In the scenario where the SSE is not stable at the reductive potential of Li metal, then this 2-dimensional interface will result in much less SEI formation compared to an anode composite. Li metal does not need to be mixed with SSE because it is already a good ion and electron conductor. Similarly, many alloy anodes such as Si also exhibit adequate ionic and electronic conductivities [25]. As such, these alloys can be used without forming a composite with SSE or carbon additives. Aside from limiting SSE reduction and the resulting Li^+ consumption, these metallic anodes can enable higher energy densities due to their high specific capacities [25] and the lack of inactive SSE and carbon components. It is important to note that zero SEI formation would still be ideal, as it would not consume any of the Li^+ inventory. However, practical materials stable at 0 V vs Li/Li^+ remain elusive. Previously, some materials have been thought to be electrochemically stable at this low reduction potential, but the cycling performance was still limited, indicating a possible oversight in the assessment of the electrochemical stability of SSEs.

4 Electrochemical Characterization Tools

4.1 Voltammetry Measurements

First reported in 2011, LGPS demonstrated a remarkably high lithium ionic conductivity of 12 mS cm^{-1} at room temperature, surpassing those of some liquid organic electrolytes for the first time. LGPS also experimentally exhibited electrochemical stability over a wide potential window (0 – 5 V vs Li/Li^+) [1]. Despite its high ionic conductivity and supposed wide electrochemical window, LGPS (and its analogues like $Li_{10}SiPS_2S_{12}$) still displayed significant capacity fading (<80% capacity retention over 100 cycles) when it was used in the cathode composite and separator layer, even when paired with alumina-coated $Li(Ni_{1/3}Mn_{1/3}Co_{1/3})O_2$ cathode particles, and a Li metal foil anode [14]. First principles studies later revealed the metastability of LGPS, showing

that it is neither stable against reduction at low anodic potentials nor oxidation at high cathodic potentials, and was found to reduce at 1.71 V vs Li/Li^+ and oxidize at 2.15 V vs Li/Li^+ [110].

In 2016, it was shown that the experimentally reported wider stability windows of most solid electrolytes, such as LGPS and LLZO, were due to the experimental cell configuration used, which resulted in limited contact between the solid electrolyte and the semi-blocking electrode [89]. This setup, often referred to as the semi-blocking planar electrode design (for instance, Li | LGPS | Pt), is shown in Figure 6a. This limited contact area leads to very small decomposition currents which are not well-resolved from cyclic voltammetry measurements commonly collected between 0 – 5 V vs Li/Li^+. To remedy this, a new composite design was proposed, where the solid electrolyte material of interest is mixed with carbon (Li | LGPS | LGPS-C), as shown in Figure 6b. This method provides more pathways for electron transfer from the electrode to and from the SSE, which amplifies the oxidation and reduction peak currents. This allowed for the intrinsic electrochemical stability to be more accurately measured, matching first principles computational results for the first time [89]. Additionally, the amount, type, and degree of carbon mixing dramatically influences the reaction kinetics of SSEs, therefore indicating that the carbon morphology and distribution must be carefully considered to conduct proper measurements. However, many recent reports of other solid electrolyte materials, such as halide and hydride electrolytes, have continued to misrepresent their electrochemical stability by still using the metal semi-blocking planar electrode method [75,111–118]. Here, we emphasize the importance of utilizing a composite electrode design, because it has been demonstrated to be the more accurate method to experimentally evaluate the electrochemical stability window of solid electrolytes. As the number of new and exciting solid electrolytes continues to rapidly grow, it is imperative that proper measurements are conducted so that future efforts are not misguided by misleading experimental results.

4.2 Separating Charge Transfer Contributions

Just like conventional liquid electrolytes in lithium-ion batteries, solid electrolytes allow the passage of charge carrying ions but block electron transport between the anode and cathode, preventing internal shorting. However, in practice, solid electrolytes can conduct both cations and electrons to varying degrees. When both contributions are contributing to charge transfer significantly, the materials are referred to as mixed ionic-electronic conductors (MIECs). An example of a solid electrolyte exhibiting mixed conduction, shown in Figure 6c-e, illustrates the importance of cell architecture design when conducting variable frequency alternating current (AC) impedance measurements. A proper cell configuration for an ideal electrolyte, which is a good ion conductor and poor electron conductor, consists of an ionically blocking but electronically conductive material placed in contact on both sides of the solid electrolyte layer, such as carbon or Ti electrodes. This configuration can be represented, or modeled, by the Debye equivalent circuit, which consists of a resistor (R_i) in series with a capacitor (C_{int}), both of which are in parallel with another capacitor (C_{geo}), which has been previously described in literature [119]. In the case of a mixed conductor, without additional electronically blocking interfaces, both ions and electrons will contribute to charge transport across the cell, where electrons will “leak” through the solid electrolyte layer. As a result, if the electronic resistance is significantly lower than the ionic resistance, electronic transport will dominate the electrical circuit, causing the

capacitive tail associated with ion charge transfer to disappear, as demonstrated in Figure 6d. Additionally, if the material of interest is a mixed conductor in which the electrons and ions both contribute equally to the overall conduction, then the corresponding electrochemical impedance spectroscopy (EIS) spectra will exhibit two consecutive semicircles, as discussed previously [119]. To remedy this effect, an electron blocking layer (i.e., an ideal solid electrolyte) should be placed on either side of the mixed conductor, therefore preventing electron leakage, and allowing for the ionic contribution to dominate the charge transfer, which can be evidenced by the presence or reappearance of the expected capacitive tail in the Nyquist plot. However, this is yet to be a common practice in literature reporting of solid electrolyte data, potentially causing misinterpretations of electrochemical properties studied. Caution also needs to be taken when working with materials that can contain more than one ionically conducting species, such as protons, as these may also be responsible for a significant contribution to the measured ionic conductivity.

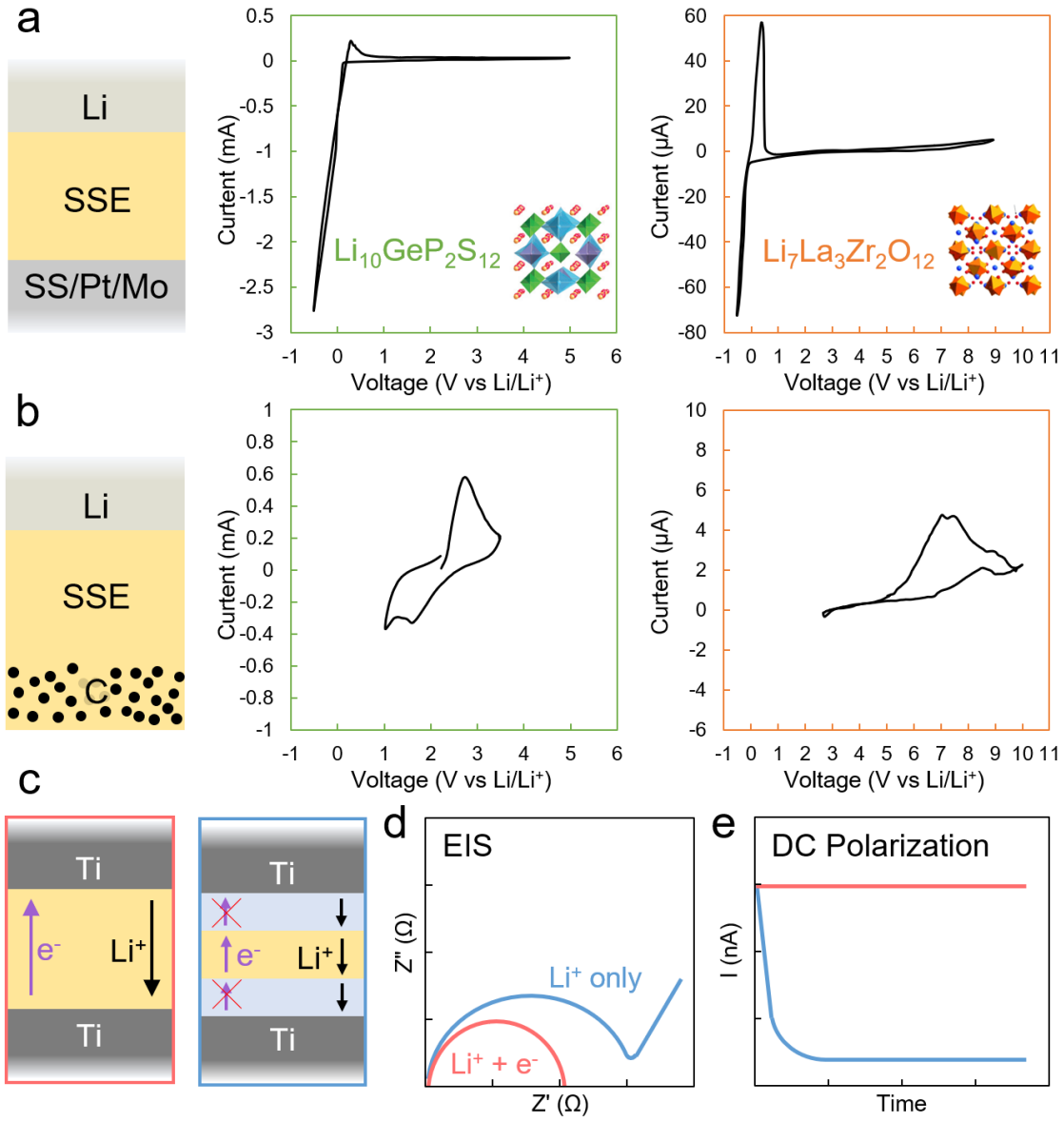

Figure 6. Measuring thermodynamic stability and electronic and ionic transport properties of SSEs. Cyclic voltammetry using **a)** planar current collectors and **b)** carbon composite electrodes for LGPS and LLZO SSEs (Contains data previously presented in [1,89]). A schematic of each setup is shown for reference. **c)** Comparison of two cell configurations on transport property measurements with mixed conductors. For mixed conductors, electron-blocking layers are needed, as demonstrated by the example **d)** EIS spectra and **e)** DC polarization measurements.

Furthermore, it is essential to complement AC impedance measurements with other techniques like direct current (DC) polarization to isolate charge transfer contributions from electrons. This ensures that the ionic conductivity value determined by EIS represents only ionic charge transfer contributions. Here, a solid electrolyte layer is surrounded by an ionically-blocking but electronically-conducting material, where a low to moderate bias (~ 50 mV – 1V) is applied across the solid electrolyte layer and the current response is measured over time (Figure 6e). Initially, both ion and electron transport will contribute to charge transfer and the subsequent measured current response, but over time the measured current will decrease since the ionically blocking electrodes cannot supply ions to the system, resulting in only electrons that contribute to the measured current response [120]. Therefore, proper cell configurations for AC impedance measurements, in tandem with DC polarization measurements, can be used to separate and accurately assess the ionic and electronic contributions to the overall charge transfer. Appropriate experimental characterization of ionic and electronic transport properties, in addition to intrinsic thermodynamic stability measurements, will help to screen the abundance of newly discovered solid electrolytes and facilitate the development of solid-state battery technologies. Moreover, with the electrochemical evaluation of solid electrolytes properly addressed, the focus in the research community can freely shift towards the remaining challenges regarding the long-term cycling performance of ASSBs. Even when using stable or passivating SSEs, capacity fade can still be observed, indicating the presence of additional failure mechanisms, such as mechanical and pressure effects, as previously discussed.

5 Conclusion and Future Perspective

A survey of the current ASSB literature has clearly shown that charge transport and mechanical properties are essential factors influencing the performance of ASSBs. Historically, the main bottleneck for enabling ASSBs were low room temperature ionic conductivities of SSEs. However, this is no longer the case, as many highly conducting and chemically compatible SSEs have been reported in the literature. Therefore, we believe that the focus should now shift toward the most pressing and remaining challenges, such as understanding and optimizing the charge transport capabilities of cathode composites to enable high areal capacities with reasonable current densities. This includes balancing cathode and SSE particle sizes, as the SSE particles should be sufficiently smaller than the cathode particles to ensure the highest utilization of the active material, while reducing SSE loading in the composite. Additionally, new strategies are needed for utilizing carbon additives that enable sufficient electron transport to the cathode particles, while minimizing transport to the SSE to limit electrolyte oxidation. To achieve commercially relevant cell performance, cathode composites should be intentionally designed to meet certain particle size and component ratios based on systematic studies and optimization. Furthermore, a proper understanding of electrochemical and charge transfer measurements is critical, particularly with

mixed conductors. Thoughtful experiments can be designed and conducted to better quantify these parameters in order to enable higher areal loadings and current densities.

A shift in focus towards mechanical aspects of ASSB cell design is also urgently needed. As Li^+ is shuttled between the electrodes, both the cathode and anode will experience volume change. While volume change associated with the cathode can result in the formation of voids and increased cell polarization, we believe this can be solved through strategies including cathode microstructure design as well as combining multiple cathode materials that undergo opposing volume changes.

Understanding the mechanical aspects remains a challenge at the anode side. While much excitement has been generated in recent years about Li metal anodes being the "holy grail" of Li-ion batteries, the volume change associated with plating Li metal presents a significant challenge for all-solid-state cell designs. We predict that this will be one of the biggest hurdles to the commercialization of ASSBs. This challenge is even more significant when designing Na-ASSB systems as Na metal will result in ~60% more cell volume expansion compared to Li metal (8 μm vs 5 μm per mAh cm^{-2}). However, we do believe that it is possible to overcome such challenges through engineering, like the use of spring- or hydraulic-based cell fixtures, which can maintain constant stack pressure during cycling. If constant pressure is maintained, then the mechanical shorting challenge can be solved. Moreover, increased attention should be paid to cell design considerations, and we expect that new tools such as machine learning and ASSB modeling will play an increasingly important role in enabling practical ASSB cells, as they have previously for traditional Li-ion batteries. After addressing these transport and mechanical challenges, solid-state batteries will deliver on their promises of safer, higher energy density, and longer lasting batteries.

6 Acknowledgements

Funding to support this work was provided by LG Energy Solutions through the Battery Innovation Contest (BIC) and Global Innovation Contest programs. Additional support was provided by the National Science Foundation through the Partnerships for Innovation (PFI) grant No. 2044465.

References:

[1] N. Kamaya, K. Homma, Y. Yamakawa, M. Hirayama, R. Kanno, M. Yonemura, T. Kamiyama, Y. Kato, S. Hama, K. Kawamoto, A. Mitsui, A lithium superionic conductor, Nature Mater. 10 (2011) 682–686. https://doi.org/10.1038/nmat3066.

[2] A. Hayashi, N. Masuzawa, S. Yubuchi, F. Tsuji, C. Hotehama, A. Sakuda, M. Tatsumisago, A sodium-ion sulfide solid electrolyte with unprecedented conductivity at room temperature, Nat Commun. 10 (2019) 5266. https://doi.org/10.1038/s41467-019-13178-2.

[3] A. Banerjee, K.H. Park, J.W. Heo, Y.J. Nam, C.K. Moon, S.M. Oh, S.-T. Hong, Y.S. Jung, Na3SbS4: A Solution Processable Sodium Superionic Conductor for All-Solid-State Sodium-Ion Batteries, Angewandte Chemie. 128 (2016) 9786–9790. https://doi.org/10.1002/ange.201604158.

[4] Y. Seino, T. Ota, K. Takada, A. Hayashi, M. Tatsumisago, A sulphide lithium super ion conductor is superior to liquid ion conductors for use in rechargeable batteries, Energy Environ. Sci. 7 (2014) 627–631. https://doi.org/10.1039/C3EE41655K.

[5] Z. Yu, S.-L. Shang, J.-H. Seo, D. Wang, X. Luo, Q. Huang, S. Chen, J. Lu, X. Li, Z.-K. Liu, D. Wang, Exceptionally High Ionic Conductivity in Na3P0.62As0.38S4 with Improved Moisture Stability for Solid-State Sodium-Ion Batteries, Advanced Materials. 29 (2017) 1605561. https://doi.org/10.1002/adma.201605561.

[6] Y. Kato, S. Hori, T. Saito, K. Suzuki, M. Hirayama, A. Mitsui, M. Yonemura, H. Iba, R. Kanno, High-power all-solid-state batteries using sulfide superionic conductors, Nat Energy. 1 (2016) 1–7. https://doi.org/10.1038/nenergy.2016.30.

[7] P. Goharian, B. Eftekhari Yekta, A.R. Aghaei, S. Banijamali, Lithium ion-conducting glass-ceramics in the system Li2O–TiO2–P2O5–Cr2O3–SiO2, Journal of Non-Crystalline Solids. 409 (2015) 120–125. https://doi.org/10.1016/j.jnoncrysol.2014.11.016.

[8] M.H. Braga, J.A. Ferreira, V. Stockhausen, J.E. Oliveira, A. El-Azab, Novel Li3ClO based glasses with superionic properties for lithium batteries, J. Mater. Chem. A. 2 (2014) 5470–5480. https://doi.org/10.1039/C3TA15087A.

[9] Y. Li, W. Zhou, X. Chen, X. Lü, Z. Cui, S. Xin, L. Xue, Q. Jia, J.B. Goodenough, Mastering the interface for advanced all-solid-state lithium rechargeable batteries, PNAS. 113 (2016) 13313–13317. https://doi.org/10.1073/pnas.1615912113.

[10] H. Xu, Y. Li, A. Zhou, N. Wu, S. Xin, Z. Li, J.B. Goodenough, Li3N-Modified Garnet Electrolyte for All-Solid-State Lithium Metal Batteries Operated at 40 °C, Nano Lett. 18 (2018) 7414–7418. https://doi.org/10.1021/acs.nanolett.8b03902.

[11] Y. Aihara, S. Ito, R. Omoda, T. Yamada, S. Fujiki, T. Watanabe, Y. Park, S. Doo, The Electrochemical Characteristics and Applicability of an Amorphous Sulfide-Based Solid Ion Conductor for the Next-Generation Solid-State Lithium Secondary Batteries, Front. Energy Res. 4 (2016). https://doi.org/10.3389/fenrg.2016.00018.

[12] M. Kotobuki, H. Munakata, K. Kanamura, Y. Sato, T. Yoshida, Compatibility of Li7La3Zr2O12 Solid Electrolyte to All-Solid-State Battery Using Li Metal Anode, J. Electrochem. Soc. 157 (2010) A1076. https://doi.org/10.1149/1.3474232.

[13] S. Randau, D.A. Weber, O. Kötz, R. Koerver, P. Braun, A. Weber, E. Ivers-Tiffée, T. Adermann, J. Kulisch, W.G. Zeier, F.H. Richter, J. Janek, Benchmarking the performance of all-solid-state lithium batteries, Nature Energy. 5 (2020) 259–270. https://doi.org/10.1038/s41560-020-0565-1.

[14] J.M. Whiteley, J.H. Woo, E. Hu, K.-W. Nam, S.-H. Lee, Empowering the Lithium Metal Battery through a Silicon-Based Superionic Conductor, J. Electrochem. Soc. 161 (2014) A1812–A1817. https://doi.org/10.1149/2.0501412jes.

[15] Z. Zhang, S. Chen, J. Yang, J. Wang, L. Yao, X. Yao, P. Cui, X. Xu, Interface Re-Engineering of Li10GeP2S12 Electrolyte and Lithium anode for All-Solid-State Lithium Batteries with Ultralong Cycle Life, ACS Appl. Mater. Interfaces. 10 (2018) 2556–2565. https://doi.org/10.1021/acsami.7b16176.

[16] J.H. Woo, J.E. Trevey, A.S. Cavanagh, Y.S. Choi, S.C. Kim, S.M. George, K.H. Oh, S.-H. Lee, Nanoscale Interface Modification of $LiCoO_2$ by Al_2O_3 Atomic Layer Deposition for Solid-State Li Batteries, J. Electrochem. Soc. 159 (2012) A1120–A1124. https://doi.org/10.1149/2.085207jes.

[17] D. Xie, S. Chen, Z. Zhang, J. Ren, L. Yao, L. Wu, X. Yao, X. Xu, High ion conductive Sb2O5-doped β-Li3PS4 with excellent stability against Li for all-solid-state lithium batteries, Journal of Power Sources. 389 (2018) 140–147.

[18] S.-J. Choi, S.-H. Choi, A.D. Bui, Y.-J. Lee, S.-M. Lee, H.-C. Shin, Y.-C. Ha, LiI-Doped Sulfide Solid Electrolyte: Enabling a High-Capacity Slurry-Cast Electrode by Low-Temperature Post-Sintering for Practical All-Solid-State Lithium Batteries, ACS Appl. Mater. Interfaces. 10 (2018) 31404–31412. https://doi.org/10.1021/acsami.8b11244.

[19] T. Yamada, S. Ito, R. Omoda, T. Watanabe, Y. Aihara, M. Agostini, U. Ulissi, J. Hassoun, B. Scrosati, All Solid-State Lithium–Sulfur Battery Using a Glass-Type P2S5–Li2S Electrolyte: Benefits on Anode Kinetics, J. Electrochem. Soc. 162 (2015) A646. https://doi.org/10.1149/2.0441504jes.

[20] M. Finsterbusch, T. Danner, C.-L. Tsai, S. Uhlenbruck, A. Latz, O. Guillon, High Capacity Garnet-Based All-Solid-State Lithium Batteries: Fabrication and 3D-Microstructure Resolved Modeling, ACS Appl. Mater. Interfaces. 10 (2018) 22329–22339. https://doi.org/10.1021/acsami.8b06705.

[21] X. Yao, D. Liu, C. Wang, P. Long, G. Peng, Y.-S. Hu, H. Li, L. Chen, X. Xu, High-Energy All-Solid-State Lithium Batteries with Ultralong Cycle Life, Nano Lett. 16 (2016) 7148–7154. https://doi.org/10.1021/acs.nanolett.6b03448.

[22] M.-S. Park, Y.-C. Jung, D.-W. Kim, Hybrid solid electrolytes composed of poly(1,4-butylene adipate) and lithium aluminum germanium phosphate for all-solid-state Li/LiNi0.6Co0.2Mn0.2O2 cells, Solid State Ionics. 315 (2018) 65–70. https://doi.org/10.1016/j.ssi.2017.12.007.

[23] T. Ates, M. Keller, J. Kulisch, T. Adermann, S. Passerini, Development of an all-solid-state lithium battery by slurry-coating procedures using a sulfidic electrolyte, Energy Storage Materials. 17 (2019) 204–210. https://doi.org/10.1016/j.ensm.2018.11.011.

[24] Y.-G. Lee, S. Fujiki, C. Jung, N. Suzuki, N. Yashiro, R. Omoda, D.-S. Ko, T. Shiratsuchi, T. Sugimoto, S. Ryu, J.H. Ku, T. Watanabe, Y. Park, Y. Aihara, D. Im, I.T. Han, High-energy long-cycling all-solid-state lithium metal batteries enabled by silver–carbon composite anodes, Nature Energy. 5 (2020) 299–308. https://doi.org/10.1038/s41560-020-0575-z.

[25] D.H.S. Tan, Y.-T. Chen, H. Yang, W. Bao, B. Sreenarayanan, J.-M. Doux, W. Li, B. Lu, S.-Y. Ham, B. Sayahpour, J. Scharf, E.A. Wu, G. Deysher, H.E. Han, H.J. Hah, H. Jeong, Z. Chen, Y.S. Meng, Carbon Free High Loading Silicon Anodes Enabled by Sulfide Solid Electrolytes for Robust All Solid-State Batteries, ArXiv:2103.04230 [Cond-Mat, Physics:Physics]. (2021). http://arxiv.org/abs/2103.04230 (accessed August 18, 2021).

[26] L. Wu, G. Liu, H. Wan, W. Weng, X. Yao, Superior lithium-stable Li7P2S8I solid electrolyte for all-solid-state lithium batteries, Journal of Power Sources. 491 (2021) 229565. https://doi.org/10.1016/j.jpowsour.2021.229565.
[27] W. Xiao, H. Xu, M. Xuan, Z. Wu, Y. Zhang, X. Zhang, S. Zhang, Y. Shen, G. Shao, Stable all-solid-state battery enabled with Li6.25PS5.25Cl0.75 as fast ion-conducting electrolyte, Journal of Energy Chemistry. 53 (2021) 147–154. https://doi.org/10.1016/j.jechem.2020.04.062.
[28] J. Duan, W. Wu, A.M. Nolan, T. Wang, J. Wen, C. Hu, Y. Mo, W. Luo, Y. Huang, Lithium–Graphite Paste: An Interface Compatible Anode for Solid-State Batteries, Advanced Materials. 31 (2019) 1807243. https://doi.org/10.1002/adma.201807243.
[29] Y. Ren, Y. Shen, Y. Lin, C.-W. Nan, Direct observation of lithium dendrites inside garnet-type lithium-ion solid electrolyte, Electrochemistry Communications. 57 (2015) 27–30. https://doi.org/10.1016/j.elecom.2015.05.001.
[30] E.J. Cheng, A. Sharafi, J. Sakamoto, Intergranular Li metal propagation through polycrystalline Li6.25Al0.25La3Zr2O12 ceramic electrolyte, Electrochimica Acta. 223 (2017). https://doi.org/10.1016/j.electacta.2016.12.018.
[31] X. Liu, R. Garcia-Mendez, A.R. Lupini, Y. Cheng, Z.D. Hood, F. Han, A. Sharafi, J.C. Idrobo, N.J. Dudney, C. Wang, C. Ma, J. Sakamoto, M. Chi, Local electronic structure variation resulting in Li 'filament' formation within solid electrolytes, Nat. Mater. (2021) 1–6. https://doi.org/10.1038/s41563-021-01019-x.
[32] Z. Zhang, L. Zhang, Y. Liu, X. Yan, B. Xu, L. Wang, One-step solution process toward formation of Li6PS5Cl argyrodite solid electrolyte for all-solid-state lithium-ion batteries, Journal of Alloys and Compounds. 812 (2020) 152103. https://doi.org/10.1016/j.jallcom.2019.152103.
[33] R. Garcia-Mendez, F. Mizuno, R. Zhang, T.S. Arthur, J. Sakamoto, Effect of Processing Conditions of 75Li2S-25P2S5 Solid Electrolyte on its DC Electrochemical Behavior, Electrochimica Acta. 237 (2017) 144–151. https://doi.org/10.1016/j.electacta.2017.03.200.
[34] Z. Zhang, L. Zhang, X. Yan, H. Wang, Y. Liu, C. Yu, X. Cao, L. van Eijck, B. Wen, All-in-one improvement toward Li6PS5Br-Based solid electrolytes triggered by compositional tune, Journal of Power Sources. 410–411 (2019) 162–170. https://doi.org/10.1016/j.jpowsour.2018.11.016.
[35] C. Wang, H. Xie, W. Ping, J. Dai, G. Feng, Y. Yao, S. He, J. Weaver, H. Wang, K. Gaskell, L. Hu, A general, highly efficient, high temperature thermal pulse toward high performance solid state electrolyte, Energy Storage Materials. 17 (2019) 234–241. https://doi.org/10.1016/j.ensm.2018.11.007.
[36] M. Motoyama, Y. Tanaka, T. Yamamoto, N. Tsuchimine, S. Kobayashi, Y. Iriyama, The Active Interface of Ta-Doped Li7La3Zr2O12 for Li Plating/Stripping Revealed by Acid Aqueous Etching, ACS Appl. Energy Mater. 2 (2019) 6720–6731. https://doi.org/10.1021/acsaem.9b01193.
[37] J. Liang, X. Li, Y. Zhao, L.V. Goncharova, W. Li, K.R. Adair, M.N. Banis, Y. Hu, T.-K. Sham, H. Huang, L. Zhang, S. Zhao, S. Lu, R. Li, X. Sun, An Air-Stable and Dendrite-Free Li Anode for Highly Stable All-Solid-State Sulfide-Based Li Batteries, Advanced Energy Materials. 9 (2019) 1902125. https://doi.org/10.1002/aenm.201902125.
[38] H. Huo, Y. Chen, R. Li, N. Zhao, J. Luo, J.G.P. da Silva, R. Mücke, P. Kaghazchi, X. Guo, X. Sun, Design of a mixed conductive garnet/Li interface for dendrite-free solid lithium metal batteries, Energy Environ. Sci. 13 (2020) 127–134. https://doi.org/10.1039/C9EE01903K.

[39] M. Wang, J.B. Wolfenstine, J. Sakamoto, Temperature dependent flux balance of the Li/Li7La3Zr2O12 interface, Electrochimica Acta. 296 (2019) 842–847. https://doi.org/10.1016/j.electacta.2018.11.034.
[40] F. Flatscher, M. Philipp, S. Ganschow, H.M.R. Wilkening, D. Rettenwander, The natural critical current density limit for Li7La3Zr2O12 garnets, J. Mater. Chem. A. 8 (2020) 15782–15788. https://doi.org/10.1039/C9TA14177D.
[41] P. Bonnick, K. Niitani, M. Nose, K. Suto, T.S. Arthur, J. Muldoon, A high performance all solid state lithium sulfur battery with lithium thiophosphate solid electrolyte, J. Mater. Chem. A. 7 (2019) 24173–24179. https://doi.org/10.1039/C9TA06971B.
[42] S.P. Kammampata, H. Yamada, T. Ito, R. Paul, V. Thangadurai, The activation entropy for ionic conduction and critical current density for Li charge transfer in novel garnet-type Li6.5La2.9A0.1Zr1.4Ta0.6O12 (A = Ca, Sr, Ba) solid electrolytes, J. Mater. Chem. A. 8 (2020) 2581–2590. https://doi.org/10.1039/C9TA12193E.
[43] F.M. Pesci, R.H. Brugge, A.K.O. Hekselman, A. Cavallaro, R.J. Chater, A. Aguadero, Elucidating the role of dopants in the critical current density for dendrite formation in garnet electrolytes, J. Mater. Chem. A. 6 (2018) 19817–19827. https://doi.org/10.1039/C8TA08366E.
[44] B. Xu, W. Li, H. Duan, H. Wang, Y. Guo, H. Li, H. Liu, Li3PO4-added garnet-type Li6.5La3Zr1.5Ta0.5O12 for Li-dendrite suppression, Journal of Power Sources. 354 (2017) 68–73. https://doi.org/10.1016/j.jpowsour.2017.04.026.
[45] F.J.Q. Cortes, J.A. Lewis, J. Tippens, T.S. Marchese, M.T. McDowell, How Metallic Protection Layers Extend the Lifetime of NASICON-Based Solid-State Lithium Batteries, J. Electrochem. Soc. 167 (2019) 050502. https://doi.org/10.1149/2.0032005JES.
[46] H. Zhong, L. Sang, F. Ding, J. Song, Y. Mai, Conformation of lithium-aluminium alloy interphase-layer on lithium metal anode used for solid state batteries, Electrochimica Acta. 277 (2018) 268–275. https://doi.org/10.1016/j.electacta.2018.04.191.
[47] N. Delaporte, A. Guerfi, H. Demers, H. Lorrmann, A. Paolella, K. Zaghib, Facile Protection of Lithium Metal for All-Solid-State Batteries, ChemistryOpen. 8 (2019) 192–195. https://doi.org/10.1002/open.201900021.
[48] T. Deng, X. Ji, Y. Zhao, L. Cao, S. Li, S. Hwang, C. Luo, P. Wang, H. Jia, X. Fan, X. Lu, D. Su, X. Sun, C. Wang, J.-G. Zhang, Tuning the Anode–Electrolyte Interface Chemistry for Garnet-Based Solid-State Li Metal Batteries, Advanced Materials. 32 (2020) 2000030. https://doi.org/10.1002/adma.202000030.
[49] S. Choi, S. Lee, J. Yu, C.-H. Doh, Y.-C. Ha, Slurry-Processed Glass-Ceramic LI2S-P2S5-LiI Electrolyte for All-Solid-State Li-Ion Batteries, ECS Trans. 77 (2017) 65. https://doi.org/10.1149/07701.0065ecst.
[50] F. Han, J. Yue, X. Zhu, C. Wang, Suppressing Li Dendrite Formation in Li2S-P2S5 Solid Electrolyte by LiI Incorporation, Advanced Energy Materials. 8 (2018) 1703644. https://doi.org/10.1002/aenm.201703644.
[51] J. Wen, Y. Huang, J. Duan, Y. Wu, W. Luo, L. Zhou, C. Hu, L. Huang, X. Zheng, W. Yang, Z. Wen, Y. Huang, Highly Adhesive Li-BN Nanosheet Composite Anode with Excellent Interfacial Compatibility for Solid-State Li Metal Batteries, ACS Nano. 13 (2019) 14549–14556. https://doi.org/10.1021/acsnano.9b08803.
[52] X. Fan, X. Ji, F. Han, J. Yue, J. Chen, L. Chen, T. Deng, J. Jiang, C. Wang, Fluorinated solid electrolyte interphase enables highly reversible solid-state Li metal battery, Science Advances. 4 (2018) eaau9245. https://doi.org/10.1126/sciadv.aau9245.

[53] Y. Su, L. Ye, W. Fitzhugh, Y. Wang, E. Gil-González, I. Kim, X. Li, A more stable lithium anode by mechanical constriction for solid state batteries, Energy Environ. Sci. 13 (2020) 908–916. https://doi.org/10.1039/C9EE04007B.
[54] L. Cheng, W. Chen, M. Kunz, K. Persson, N. Tamura, G. Chen, M. Doeff, Effect of Surface Microstructure on Electrochemical Performance of Garnet Solid Electrolytes, ACS Appl. Mater. Interfaces. 7 (2015) 2073–2081. https://doi.org/10.1021/am508111r.
[55] A. Sharafi, H.M. Meyer, J. Nanda, J. Wolfenstine, J. Sakamoto, Characterizing the Li–Li7La3Zr2O12 interface stability and kinetics as a function of temperature and current density, Journal of Power Sources. 302 (2016) 135–139. https://doi.org/10.1016/j.jpowsour.2015.10.053.
[56] X. Han, Y. Gong, K. (Kelvin) Fu, X. He, G.T. Hitz, J. Dai, A. Pearse, B. Liu, H. Wang, G. Rubloff, Y. Mo, V. Thangadurai, E.D. Wachsman, L. Hu, Negating interfacial impedance in garnet-based solid-state Li metal batteries, Nature Materials. 16 (2017) 572–579. https://doi.org/10.1038/nmat4821.
[57] A. Sharafi, E. Kazyak, A.L. Davis, S. Yu, T. Thompson, D.J. Siegel, N.P. Dasgupta, J. Sakamoto, Surface Chemistry Mechanism of Ultra-Low Interfacial Resistance in the Solid-State Electrolyte Li7La3Zr2O12, Chem. Mater. 29 (2017) 7961–7968. https://doi.org/10.1021/acs.chemmater.7b03002.
[58] A. Sharafi, C.G. Haslam, R.D. Kerns, J. Wolfenstine, J. Sakamoto, Controlling and correlating the effect of grain size with the mechanical and electrochemical properties of Li7La3Zr2O12 solid-state electrolyte, J. Mater. Chem. A. 5 (2017) 21491–21504. https://doi.org/10.1039/C7TA06790A.
[59] J. Kasemchainan, S. Zekoll, D. Spencer Jolly, Z. Ning, G.O. Hartley, J. Marrow, P.G. Bruce, Critical stripping current leads to dendrite formation on plating in lithium anode solid electrolyte cells, Nature Materials. 18 (2019) 1105–1111. https://doi.org/10.1038/s41563-019-0438-9.
[60] C. Wang, Y. Gong, J. Dai, L. Zhang, H. Xie, G. Pastel, B. Liu, E. Wachsman, H. Wang, L. Hu, In Situ Neutron Depth Profiling of Lithium Metal–Garnet Interfaces for Solid State Batteries, J. Am. Chem. Soc. 139 (2017) 14257–14264. https://doi.org/10.1021/jacs.7b07904.
[61] W. Tang, S. Tang, X. Guan, X. Zhang, Q. Xiang, J. Luo, High-Performance Solid Polymer Electrolytes Filled with Vertically Aligned 2D Materials, Advanced Functional Materials. 29 (2019) 1900648. https://doi.org/10.1002/adfm.201900648.
[62] R. Schlenker, D. Stępień, P. Koch, T. Hupfer, S. Indris, B. Roling, V. Miß, A. Fuchs, M. Wilhelmi, H. Ehrenberg, Understanding the Lifetime of Battery Cells Based on Solid-State Li6PS5Cl Electrolyte Paired with Lithium Metal Electrode, ACS Appl. Mater. Interfaces. 12 (2020) 20012–20025. https://doi.org/10.1021/acsami.9b22629.
[63] Y. Xiao, Y. Wang, S.-H. Bo, J.C. Kim, L.J. Miara, G. Ceder, Understanding interface stability in solid-state batteries, Nat Rev Mater. 5 (2020) 105–126. https://doi.org/10.1038/s41578-019-0157-5.
[64] C. Wang, J. Hong, Ionic/Electronic Conducting Characteristics of LiFePO4 Cathode Materials: The Determining Factors for High Rate Performance, Electrochem. Solid-State Lett. 10 (2007) A65. https://doi.org/10.1149/1.2409768.
[65] J. Hong, C. Wang, U. Kasavajjula, Kinetic behavior of LiFeMgPO4 cathode material for Li-ion batteries, Journal of Power Sources. 162 (2006) 1289–1296. https://doi.org/10.1016/j.jpowsour.2006.08.004.

[66] A. Bielefeld, D.A. Weber, J. Janek, Microstructural Modeling of Composite Cathodes for All-Solid-State Batteries, J. Phys. Chem. C. 123 (2019) 1626–1634. https://doi.org/10.1021/acs.jpcc.8b11043.
[67] T. Shi, Q. Tu, Y. Tian, Y. Xiao, L.J. Miara, O. Kononova, G. Ceder, High Active Material Loading in All-Solid-State Battery Electrode via Particle Size Optimization, Advanced Energy Materials. 10 (2020) 1902881. https://doi.org/10.1002/aenm.201902881.
[68] G.F. Dewald, S. Ohno, J.G.C. Hering, J. Janek, W.G. Zeier, Analysis of Charge Carrier Transport Toward Optimized Cathode Composites for All-Solid-State Li−S Batteries, Batteries & Supercaps. 4 (2021) 183–194. https://doi.org/10.1002/batt.202000194.
[69] W. Zhang, T. Leichtweiß, S.P. Culver, R. Koerver, D. Das, D.A. Weber, W.G. Zeier, J. Janek, The Detrimental Effects of Carbon Additives in Li10GeP2S12-Based Solid-State Batteries, ACS Appl. Mater. Interfaces. 9 (2017) 35888–35896. https://doi.org/10.1021/acsami.7b11530.
[70] KETJENBLACK Highly Electro-Conductive Carbon Black | Lion Specialty Chemicals Co., Ltd., (n.d.). https://www.lion-specialty-chem.co.jp/en/product/carbon/carbon01.htm (accessed July 11, 2021).
[71] D.H.S. Tan, E.A. Wu, H. Nguyen, Z. Chen, M.A.T. Marple, J.-M. Doux, X. Wang, H. Yang, A. Banerjee, Y.S. Meng, Elucidating Reversible Electrochemical Redox of Li6PS5Cl Solid Electrolyte, ACS Energy Lett. 4 (2019) 2418–2427. https://doi.org/10.1021/acsenergylett.9b01693.
[72] A. Banerjee, X. Wang, C. Fang, E.A. Wu, Y.S. Meng, Interfaces and Interphases in All-Solid-State Batteries with Inorganic Solid Electrolytes, Chem. Rev. 120 (2020) 6878–6933. https://doi.org/10.1021/acs.chemrev.0c00101.
[73] W.D. Richards, L.J. Miara, Y. Wang, J.C. Kim, G. Ceder, Interface Stability in Solid-State Batteries, Chem. Mater. 28 (2016) 266–273. https://doi.org/10.1021/acs.chemmater.5b04082.
[74] Y. Han, S.H. Jung, H. Kwak, S. Jun, H.H. Kwak, J.H. Lee, S.-T. Hong, Y.S. Jung, Single- or Poly-Crystalline Ni-Rich Layered Cathode, Sulfide or Halide Solid Electrolyte: Which Will be the Winners for All-Solid-State Batteries?, Advanced Energy Materials. 11 (2021) 2100126. https://doi.org/10.1002/aenm.202100126.
[75] T. Asano, A. Sakai, S. Ouchi, M. Sakaida, A. Miyazaki, S. Hasegawa, Solid Halide Electrolytes with High Lithium-Ion Conductivity for Application in 4 V Class Bulk-Type All-Solid-State Batteries, Advanced Materials. 30 (2018) 1803075. https://doi.org/10.1002/adma.201803075.
[76] K.-H. Park, K. Kaup, A. Assoud, Q. Zhang, X. Wu, L.F. Nazar, High-Voltage Superionic Halide Solid Electrolytes for All-Solid-State Li-Ion Batteries, ACS Energy Lett. 5 (2020) 533–539. https://doi.org/10.1021/acsenergylett.9b02599.
[77] Z. Liu, S. Ma, J. Liu, S. Xiong, Y. Ma, H. Chen, High Ionic Conductivity Achieved in Li3Y(Br3Cl3) Mixed Halide Solid Electrolyte via Promoted Diffusion Pathways and Enhanced Grain Boundary, ACS Energy Lett. 6 (2021) 298–304. https://doi.org/10.1021/acsenergylett.0c01690.
[78] D.H. Kim, D.Y. Oh, K.H. Park, Y.E. Choi, Y.J. Nam, H.A. Lee, S.-M. Lee, Y.S. Jung, Infiltration of Solution-Processable Solid Electrolytes into Conventional Li-Ion-Battery Electrodes for All-Solid-State Li-Ion Batteries, Nano Lett. 17 (2017) 3013–3020. https://doi.org/10.1021/acs.nanolett.7b00330.
[79] Y.-T. Chen, M. Duquesnoy, D.H.S. Tan, J.-M. Doux, H. Yang, G. Deysher, P. Ridley, A.A. Franco, Y.S. Meng, Z. Chen, Fabrication of High-Quality Thin Solid-State Electrolyte Films

Assisted by Machine Learning, ACS Energy Lett. 6 (2021) 1639–1648. https://doi.org/10.1021/acsenergylett.1c00332.
[80] Y.J. Nam, S.-J. Cho, D.Y. Oh, J.-M. Lim, S.Y. Kim, J.H. Song, Y.-G. Lee, S.-Y. Lee, Y.S. Jung, Bendable and Thin Sulfide Solid Electrolyte Film: A New Electrolyte Opportunity for Free-Standing and Stackable High-Energy All-Solid-State Lithium-Ion Batteries, Nano Lett. 15 (2015) 3317–3323. https://doi.org/10.1021/acs.nanolett.5b00538.
[81] D.H.S. Tan, Y.-T. Chen, H. Yang, W. Bao, B. Sreenarayanan, J.-M. Doux, W. Li, B. Lu, S.-Y. Ham, B. Sayahpour, J. Scharf, E.A. Wu, G. Deysher, H.E. Han, H.J. Hah, H. Jeong, Z. Chen, Y.S. Meng, Carbon Free High Loading Silicon Anodes Enabled by Sulfide Solid Electrolytes for Robust All Solid-State Batteries, (2021). https://arxiv.org/abs/2103.04230v1 (accessed July 13, 2021).
[82] E.A. Wu, S. Banerjee, H. Tang, P.M. Richardson, J.-M. Doux, J. Qi, Z. Zhu, A. Grenier, Y. Li, E. Zhao, G. Deysher, E. Sebti, H. Nguyen, R. Stephens, G. Verbist, K.W. Chapman, R.J. Clément, A. Banerjee, Y.S. Meng, S.P. Ong, A stable cathode-solid electrolyte composite for high-voltage, long-cycle-life solid-state sodium-ion batteries, Nat Commun. 12 (2021) 1256. https://doi.org/10.1038/s41467-021-21488-7.
[83] H.W. Kwak, Y.J. Park, Li2MoO4 coated Ni-rich cathode for all-solid-state batteries, Thin Solid Films. 660 (2018) 625–630. https://doi.org/10.1016/j.tsf.2018.04.038.
[84] J.-M. Doux, H. Nguyen, D.H.S. Tan, A. Banerjee, X. Wang, E.A. Wu, C. Jo, H. Yang, Y.S. Meng, Stack Pressure Considerations for Room-Temperature All-Solid-State Lithium Metal Batteries, Advanced Energy Materials. 10 (2020) 1903253. https://doi.org/10.1002/aenm.201903253.
[85] Y. Kato, S. Hori, T. Saito, K. Suzuki, M. Hirayama, A. Mitsui, M. Yonemura, H. Iba, R. Kanno, High-power all-solid-state batteries using sulfide superionic conductors, Nature Energy. 1 (2016) 1–7. https://doi.org/10.1038/nenergy.2016.30.
[86] R. Koerver, W. Zhang, L. de Biasi, S. Schweidler, A.O. Kondrakov, S. Kolling, T. Brezesinski, P. Hartmann, W.G. Zeier, J. Janek, Chemo-mechanical expansion of lithium electrode materials – on the route to mechanically optimized all-solid-state batteries, Energy Environ. Sci. 11 (2018) 2142–2158. https://doi.org/10.1039/C8EE00907D.
[87] T. Shi, Y.-Q. Zhang, Q. Tu, Y. Wang, M. C. Scott, G. Ceder, Characterization of mechanical degradation in an all-solid-state battery cathode, Journal of Materials Chemistry A. 8 (2020) 17399–17404. https://doi.org/10.1039/D0TA06985J.
[88] S.-K. Jung, H. Gwon, S.-S. Lee, H. Kim, J.C. Lee, J.G. Chung, S.Y. Park, Y. Aihara, D. Im, Understanding the effects of chemical reactions at the cathode–electrolyte interface in sulfide based all-solid-state batteries, J. Mater. Chem. A. 7 (2019) 22967–22976. https://doi.org/10.1039/C9TA08517C.
[89] F. Han, Y. Zhu, X. He, Y. Mo, C. Wang, Electrochemical Stability of Li10 GeP2 S12 and Li7 La3 Zr2 O12 Solid Electrolytes, Advanced Energy Materials. 6 (2016) 1501590. https://doi.org/10.1002/aenm.201501590.
[90] Materials Project, (n.d.). https://materialsproject.org/ (accessed July 13, 2021).
[91] Capacity Fade in Solid-State Batteries: Interphase Formation and Chemomechanical Processes in Nickel-Rich Layered Oxide Cathodes and Lithium Thiophosphate Solid Electrolytes | Chemistry of Materials, (n.d.). https://pubs.acs.org/doi/abs/10.1021/acs.chemmater.7b00931?casa_token=5f844PakCXsAAAAA:d_iMYswDHUs-

wI_98v8VlhEiQakyFuknUhGb48Wk0H1aSwmEQnRXOuQyEBkY7_eqxdt0HfVQPL_oJHXiFA (accessed July 13, 2021).
[92] U.-H. Kim, H.-H. Ryu, J.-H. Kim, R. Mücke, P. Kaghazchi, C.S. Yoon, Y.-K. Sun, Microstructure-Controlled Ni-Rich Cathode Material by Microscale Compositional Partition for Next-Generation Electric Vehicles, Advanced Energy Materials. 9 (2019) 1803902. https://doi.org/10.1002/aenm.201803902.
[93] Y.-N. Zhou, J. Ma, E. Hu, X. Yu, L. Gu, K.-W. Nam, L. Chen, Z. Wang, X.-Q. Yang, Tuning charge–discharge induced unit cell breathing in layer-structured cathode materials for lithium-ion batteries, Nat Commun. 5 (2014) 5381. https://doi.org/10.1038/ncomms6381.
[94] X.Q. Yang, X. Sun, J. McBreen, New phases and phase transitions observed in Li1−xCoO2 during charge: in situ synchrotron X-ray diffraction studies, Electrochemistry Communications. 2 (2000) 100–103. https://doi.org/10.1016/S1388-2481(99)00155-1.
[95] L.A. de Picciotto, M.M. Thackeray, W.I.F. David, P.G. Bruce, J.B. Goodenough, Structural characterization of delithiated LiVO2, Materials Research Bulletin. 19 (1984) 1497–1506. https://doi.org/10.1016/0025-5408(84)90264-2.
[96] N. Kumada, S. Muramatu, F. Muto, N. Kinomura, S. Kikkawa, M. Koizumi, Topochemical reactions of LixNbO2, Journal of Solid State Chemistry. 73 (1988) 33–39. https://doi.org/10.1016/0022-4596(88)90050-3.
[97] T. Ohzuku, A. Ueda, N. Yamamoto, Zero-Strain Insertion Material of Li [Li1 / 3Ti5 / 3] O 4 for Rechargeable Lithium Cells, J. Electrochem. Soc. 142 (1995) 1431. https://doi.org/10.1149/1.2048592.
[98] J.-M. Doux, H. Nguyen, D.H.S. Tan, A. Banerjee, X. Wang, E.A. Wu, C. Jo, H. Yang, Y.S. Meng, Stack Pressure Considerations for Room-Temperature All-Solid-State Lithium Metal Batteries, Advanced Energy Materials. 10 (2020) 1903253. https://doi.org/10.1002/aenm.201903253.
[99] S. Ding, L. Fairgrieve-Park, O. Sendetskyi, M.D. Fleischauer, Compressive creep deformation of lithium foil at varied cell conditions, Journal of Power Sources. 488 (2021) 229404. https://doi.org/10.1016/j.jpowsour.2020.229404.
[100] O.D. Sherby, P.M. Burke, Mechanical behavior of crystalline solids at elevated temperature, Progress in Materials Science. 13 (1968) 323–390. https://doi.org/10.1016/0079-6425(68)90024-8.
[101] M.D. Mathew, H. Yang, S. Movva, K.L. Murty, Creep deformation characteristics of tin and tin-based electronic solder alloys, Metall Mater Trans A. 36 (2005) 99–105. https://doi.org/10.1007/s11661-005-0142-z.
[102] H. Okamoto, Li-Si (Lithium-Silicon), J. Phase Equilib. Diffus. 30 (2009) 118–119. https://doi.org/10.1007/s11669-008-9431-8.
[103] B. Predel, Li-Sb (Lithium-Antimony), in: O. Madelung (Ed.), Li-Mg – Nd-Zr, Springer-Verlag, Berlin/Heidelberg, 1997: pp. 1–2. https://doi.org/10.1007/10522884_1924.
[104] S. Luo, Z. Wang, X. Li, X. Liu, H. Wang, W. Ma, L. Zhang, L. Zhu, X. Zhang, Growth of lithium-indium dendrites in all-solid-state lithium-based batteries with sulfide electrolytes, Nat Commun. 12 (2021) 6968. https://doi.org/10.1038/s41467-021-27311-7.
[105] M.J. Wang, R. Choudhury, J. Sakamoto, Characterizing the Li-Solid-Electrolyte Interface Dynamics as a Function of Stack Pressure and Current Density, Joule. 3 (2019) 2165–2178. https://doi.org/10.1016/j.joule.2019.06.017.
[106] J. Kasemchainan, S. Zekoll, D. Spencer Jolly, Z. Ning, G.O. Hartley, J. Marrow, P.G. Bruce, Critical stripping current leads to dendrite formation on plating in lithium anode solid

electrolyte cells, Nat. Mater. 18 (2019) 1105–1111. https://doi.org/10.1038/s41563-019-0438-9.
[107] A. Masias, N. Felten, R. Garcia-Mendez, J. Wolfenstine, J. Sakamoto, Elastic, plastic, and creep mechanical properties of lithium metal, J Mater Sci. 54 (2019) 2585–2600. https://doi.org/10.1007/s10853-018-2971-3.
[108] W.S. LePage, Y. Chen, E. Kazyak, K.-H. Chen, A.J. Sanchez, A. Poli, E.M. Arruda, M.D. Thouless, N.P. Dasgupta, Lithium Mechanics: Roles of Strain Rate and Temperature and Implications for Lithium Metal Batteries, J. Electrochem. Soc. 166 (2019) A89–A97. https://doi.org/10.1149/2.0221902jes.
[109] Hydrogen Storage - Basics, Energy.Gov. (n.d.). https://www.energy.gov/eere/fuelcells/hydrogen-storage-basics-0 (accessed January 24, 2022).
[110] Y. Zhu, X. He, Y. Mo, First principles study on electrochemical and chemical stability of solid electrolyte–electrode interfaces in all-solid-state Li-ion batteries, Journal of Materials Chemistry A. 4 (2016) 3253–3266.
[111] S. Kim, H. Oguchi, N. Toyama, T. Sato, S. Takagi, T. Otomo, D. Arunkumar, N. Kuwata, J. Kawamura, S. Orimo, A complex hydride lithium superionic conductor for high-energy-density all-solid-state lithium metal batteries, Nat Commun. 10 (2019) 1081. https://doi.org/10.1038/s41467-019-09061-9.
[112] X. Li, J. Liang, N. Chen, J. Luo, K.R. Adair, C. Wang, M.N. Banis, T. Sham, L. Zhang, S. Zhao, S. Lu, H. Huang, R. Li, X. Sun, Water-Mediated Synthesis of a Superionic Halide Solid Electrolyte, Angewandte Chemie. 131 (2019) 16579–16584. https://doi.org/10.1002/ange.201909805.
[113] Y. Lee, J. Jeong, H.-D. Lim, S.-O. Kim, H.-G. Jung, K.Y. Chung, S. Yu, Superionic Si-Substituted Lithium Argyrodite Sulfide Electrolyte Li6+xSb1–xSixS5I for All-Solid-State Batteries, ACS Sustainable Chem. Eng. 9 (2021) 120–128. https://doi.org/10.1021/acssuschemeng.0c05549.
[114] H. Jia, X. Liang, T. An, L. Peng, J. Feng, J. Xie, Effect of Halogen Doping in Sodium Solid Electrolytes Based on the Na–Sn–Si–P–S Quinary System, Chem. Mater. 32 (2020) 4065–4071. https://doi.org/10.1021/acs.chemmater.0c00872.
[115] Z. Zhang, J. Zhang, H. Jia, L. Peng, T. An, J. Xie, Enhancing ionic conductivity of solid electrolyte by lithium substitution in halogenated Li-Argyrodite, Journal of Power Sources. 450 (2020) 227601. https://doi.org/10.1016/j.jpowsour.2019.227601.
[116] J. Zhang, L. Li, C. Zheng, Y. Xia, Y. Gan, H. Huang, C. Liang, X. He, X. Tao, W. Zhang, Silicon-Doped Argyrodite Solid Electrolyte Li6PS5I with Improved Ionic Conductivity and Interfacial Compatibility for High-Performance All-Solid-State Lithium Batteries, ACS Appl. Mater. Interfaces. 12 (2020) 41538–41545. https://doi.org/10.1021/acsami.0c11683.
[117] W. Arnold, D.A. Buchberger, Y. Li, M. Sunkara, T. Druffel, H. Wang, Halide doping effect on solvent-synthesized lithium argyrodites Li6PS5X (X= Cl, Br, I) superionic conductors, Journal of Power Sources. 464 (2020) 228158. https://doi.org/10.1016/j.jpowsour.2020.228158.
[118] A.D. Bui, S.-H. Choi, H. Choi, Y.-J. Lee, C.-H. Doh, J.-W. Park, B.G. Kim, W.-J. Lee, S.-M. Lee, Y.-C. Ha, Origin of the Outstanding Performance of Dual Halide Doped Li7P2S8X (X = I, Br) Solid Electrolytes for All-Solid-State Lithium Batteries, ACS Appl. Energy Mater. 4 (2021) 1–8. https://doi.org/10.1021/acsaem.0c02321.

[119] R.A. Huggins, Simple method to determine electronic and ionic components of the conductivity in mixed conductors a review, Ionics. 8 (2002) 300–313. https://doi.org/10.1007/bf02376083.
[120] K. Yu, R. Gu, L. Wu, H. Sun, R. Ma, L. Jin, Y. Xu, Z. Xu, X. Wei, Ionic and electronic conductivity of solid electrolyte Li0.5La0.5TiO3 doped with LiO2-SiO2-B2O3 glass, Journal of Alloys and Compounds. 739 (2018) 892–896. https://doi.org/10.1016/j.jallcom.2017.12.361.